ISSN: 2688-8645

Research on Indicator Diagram Inversion Method of Beam Pumping Unit based on Power-To-Load Transfer Coefficient

Yu Zhou, Zhewei Ye

School of Mechatronic Engineering, Southwest Petroleum University, Chengdu, China

Abstract

The suspension point indicator diagram of the beam pumping unit is an essential basis for judging the operating conditions of the pumping unit. It is common to use electrical parameters to invert the suspension point indicator diagram. However, the current methods of using electrical parameters to invert the suspension point indicator diagram have the problems of low accuracy and poor practicability. Based on this, the method of inverting the indicator diagram based on the power-to-load transfer coefficient method is proposed in this paper. The transfer coefficient of power-to-load is calibrated by measured instantaneous output power of the motor and suspension point load. Then the Fourier series is used to fit the transfer coefficient. The load is calculated by measuring the instantaneous output power of the motor, suspension point displacement, and fitted transfer coefficient and the inverse indicator diagram is obtained. The average coincidence rate of the inversion indicator diagram is 98%. This method can significantly improve the inversion accuracy and simplify the process, providing a new way for the engineering application of electrical parameter inversion indicator diagrams.

Keywords

Pumping Unit; Indicator Diagram; Motor Power; Suspension Point Load; Fourier Series Fitting.

1. Introduction

The indicator diagram is a two-dimension graph of suspension point load versus horse head position. The indicator diagram is a critical characterization of the working state of the pumping unit and downhole pump, which can be used to judge the fault state of the pumping system. Currently, most oil wells use load sensors to measure the suspension point load to obtain the indicator diagram[1]. However, load sensors generally have problems such as short life, high failure rate, and measurement error accumulated over time[2]. Therefore, the research on the indirect test technology of indicator diagrams without load sensors has been paid more and more attention.

There are many types of research on the indirect measurement of indicator diagrams without load sensors at domestic and abroad. Compared with load measurement, electrical parameter measurement has the following characteristics: high reliability, high accuracy, low installation, and maintenance cost, and comprehensive information response. The inversion of indicator diagrams through electrical parameters is a research hotspot[3].

In 1987, S.G. Gibbs et al.[4] first proposed the torque coefficient to indirectly calculate suspension point load by measuring motor speed and mechanical characteristics. Li et al.[5] proposed a method to predict the indicator diagram using the pumping unit's measured motor power. Still, the position of the dead point of the suspension point must be estimated, leading to decreased load calculation accuracy. Because the torque coefficient method does not converge, mathematical techniques are applied to smooth the dead point area of the indicator diagram, such as the five-spot triple smoothing method, the limit of torque coefficient at the dead point, etc.[6,7]. Based on previous studies, Chen et al.[8] carried out an accurate dynamic analysis of the pumping unit system, established an optimization model of suspension point load and electric power, and improved the fitting accuracy of the indicator diagram. Lu et al.[9] showed a more accurate mathematical model of electric power inversion of polished rod load. This model considers pumping unit transmission efficiency, beam swing angle, and motor speed. Yin et al.[10] analyzed the power loss of each part of the pumping unit, calculated the relationship between the transmission efficiency and the crank angle by the principle of energy conservation to correct the power loss of the transmission link, and then established the mathematical model of load and displacement of the suspension point.

In recent years, with the development of artificial intelligence technology, some scholars have also integrated artificial intelligence algorithms into using electrical parameters to invert indicator diagrams. Wei et al.[11] proposed a method of electrical parameter inversion of suspension point indicator diagram based on hybrid modeling. Firstly, the mechanism model is used to calculate the suspension point load roughly, and then the extreme learning machine model is used to learn the inversion error and correct it. References[12-16] used data-driven algorithms to establish a neural network model by learning training data and mapping the measured electric power of the pumping unit to the suspension point load to achieve an indirect measurement of load.

The above methods of using electrical parameters to invert indicator diagrams have strict working conditions, and great technical limitations exist in practice and application. These methods are difficult to extend to most oil fields. Because the mathematical model of calculating the suspension point load from the electrical parameters is established by the transmission relationship and mechanical relationship of the pumping unit, many parameters need to be measured. For example, the length of the four-bar linkage of the pumping unit, the mass and moment of inertia of the moving member, the acceleration, the balance mass, and other parameters need to be measured. These steps will significantly increase the workload, and the calculation accuracy is low. Although the data-driven algorithm can theoretically improve the accuracy of the indicator diagram inversion, it requires a large amount of training data to establish a learning model, which is not practical in many cases.

Therefore, to avoid measuring too many pumping unit parameters, reduce the workload, and improve the efficiency of indicator diagram inversion, this paper proposes an inversion of the suspension point indicator diagram of the beam pumping unit based on the power-to-load transfer coefficient method.

2. Power-to-load Transfer Coefficient Method

2.1. Theoretical Basis of Power-to-load Transfer Coefficient

Figure 1(a) shows a structural diagram of a beam pumping unit commonly used in oil fields, and its type is CYJY10-3-53HB. The main components of the beam pumping unit are the motor, four-bar mechanism, frame and reducer, etc.

When the pumping unit runs, the motor's rotating motion is transmitted to the crankshaft through the belt and reducer. The motion of the crankshaft is further transmitted to the donkey head through the four-bar mechanism to make it move in a vertical reciprocating linear motion. The rope hanger is connected with the sucker rod string to drive the pump plunger in the pump barrel to move up and down in a straight line to achieve the purpose of pumping oil. In the upper stroke, the suspension point bears a rod and liquid column load. Motor and balance block work together to complete the liquid extraction process. In the down stroke, the sucker rod overcomes the buoyancy downward under its weight.

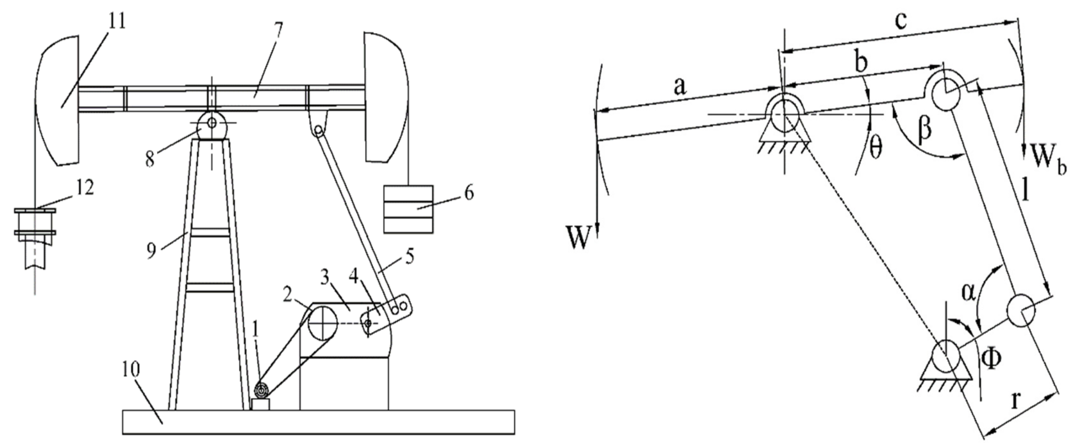

(a)Structure diagram of pumping unit (b)Simplified model of pumping unit
1-Motor ;2-Reducer pulley ;3-Reducer; 4-Crank; 5-Connecting rod; 6-Beam balance block; 7-Beam; 8-Stent shaft; 9-Stent; 10-Base; 11-Donkey head; 12-Rope hanger

Fig 1. Structure diagram and simplified model of pumping unit

According to the method in Reference[6], the pumping unit system is simplified as follows: The motor to the reducer is regarded as a constant transmission ratio transmission, ignoring the friction loss, the inertial load of the moving component, and the elastic sliding phenomenon of the belt transmission. The pumping unit is equivalent to a four-bar mechanism. The simplified results are shown in Figure 1. The static calculation model of the suspension point load of the pumping unit is shown in Equation (1).

$$W = 9550\frac{p\eta i}{\overline{TF}n\cos\theta} + B + \frac{cw_b}{a} \tag{1}$$

Where η is the transmission efficiency from the motor to the crank; P is the instantaneous motor output power, kW; i is the transmission ratio of the motor to the crank; W is the suspension point load, kN ; a is the length of the forearm,m;c is the distance from the center of mass of the balance block to the rotation center of the beam, m; $\overline{TF}$ is the pumping unit torque factor; θ is the rotation angle of the beam; B is the unbalanced weight of the pumping unit structure, kN.

The torque factor in the equation (1) is defined as follows :

$$\overline{TF} = \frac{ar\sin\alpha}{\mathrm{b}\sin\beta} \tag{2}$$

Where r is the crank length, m; b is the length of the connecting rod, m; α is the angle between the crank and connecting rod; β is the angle between the rear arm of the beam and the connecting rod.

It can be seen from the Equation (1) that the motor's instantaneous output power changes with the pumping unit's suspension point load. The changing relationship is a nonlinear function of motor efficiency, transmission efficiency, balance torque, suspension point displacement, and other parameters. However, the power transmission relationship of the pumping unit system is complex, the accuracy of the simple calculation model is low, and more parameters are needed. Based on this, for each measurement point, the ratio of the instantaneous electric power to the suspension point load is defined as the power-to-load transfer coefficient:

$$\lambda(S_i) = \frac{P_i}{W_i} \qquad i = 1,\dots,n \tag{3}$$

Where S_i is the suspension point displacement, m; P_i is the instantaneous motor output power, kW; W_i is the suspension point load, kN; $\lambda(S_i)$ is the power-to-load transfer coefficient at the ith measurement point. n is the number of measuring points of the data in a stroke of the pumping unit.

The suspension point load of $1KN$ at the measurement point i corresponds to how much power is calibrated by $\lambda(S_i)$. The calibration results imply the functional relationship between the electric power and the suspension point load, and it is a variable only related to the suspension point displacement. The balancing torque and power loss are unchanged at the same suspension point displacement in different cycles for a beam pumping unit system set with fixed operating parameters. That is to say, at the same suspension point displacement of the beam pumping unit with fixed operating parameters in different periods, the power-to-load transfer coefficient is unchanged, which is the principle of the power-to-load transfer coefficient method to invert the indicator diagram. When the indicator diagram inversion is carried out, the power-to-load transfer coefficient is calibrated by the instantaneous output power and suspension point load in a stroke of the pumping unit. Under the condition that only the instantaneous output power of the motor and the corresponding suspension point displacement is known, the related suspension point load can be inversely calculated. The calculation formula is as follows:

$$W_i' = \frac{P_i'}{\lambda(S_i)} \qquad i = 1, \ldots, n \tag{4}$$

Where W_i' is the calculated value of load inversion, kN; P_i' is the instantaneous motor output power, kW.

This method does not need to measure the structural parameters, motion parameters, and power loss of the pumping unit. It provides a straightforward new process for the engineering application of indicator diagram inversion.

2.2. Calibration of Power-to-load Transfer Coefficient

The indicator diagram data of beam pumping units in an oilfield are collected by traditional method. Two hundred measurement points are evenly collected in one stroke, and the motor's suspension point displacement, suspension point load, and instantaneous output power are collected synchronously. The acquisition object is the CYJY10-3-53 HB pumping unit in Figure 1. The measured results of a period are shown in Table 1.

Table 1. The practical measurement data of the pumping unit

Suspension point displacement(m)	Suspension point load(kN)	Motor power (kW)	Transmission coefficient
0	29.1	2.1	0.07
0	29.79	1.93	0.06
0	30.14	1.97	0.07
⋮	⋮	⋮	⋮
2.83	44.98	2.86	0.06
2.83	45.05	2.63	0.06
2.83	45.13	2.76	0.06
⋮	⋮	⋮	⋮
0	27.45	1.91	0.07

Due to beam commutation, there are repeated displacement test data at the dead point. Because the suspension point load and electric power of this part are approximately equal, the average value of the suspension point load and power in this part is taken to ensure the integrity of the displacement sequence.

After processing the data in Table 1, the indicator diagram and the power-to-load transfer coefficient curve are drawn. The drawings are shown in Figures 2 (a) and (b). Due to various complex factors such as dynamic load and friction load, the instantaneous output power of the motor and the load of the optical rod fluctuate. There are random irregular fluctuations in the indicator diagram and the power-to-load transfer coefficient, forming an irregular curve with alternating peaks and valleys.

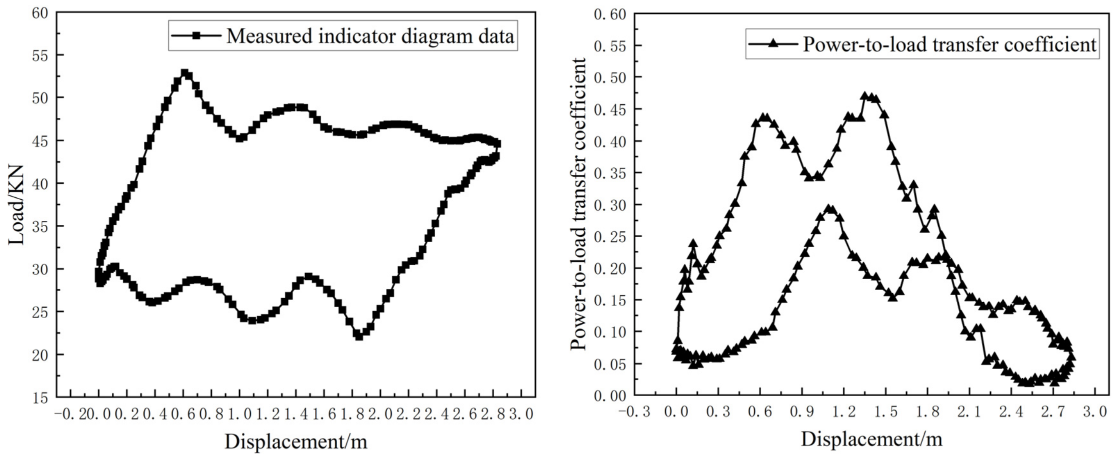

(a) Measured indicator diagram (b) The actual transfer coefficient curve

Fig 2. Measured indicator diagram and coefficient

2.3. Fitting of Power-to-load Transfer Coefficient

Only 200 points are measured in one cycle. In order to calculate the suspension point load under any displacement, the power-to-load transfer coefficient needs to be fitted by a curve.

There are many methods for curve fitting, but according to the characteristics of the coefficient curve, if the conventional fitting method is used, it is challenging to meet the fitting accuracy. References[17-19] used the Fourier series to fit the extremely irregular rock mass structural plane contour curve and achieved high fitting accuracy. Based on this, this paper selects the Fourier series function to fit the power-to-load transfer coefficient curve.

The power-to-load transfer coefficient $\lambda(S_i)$, is defined as a Fourier series function varying with the suspension point displacement S. The discrete data points of the function independent variables are $S = [S_1, S_2, \dots, S_n]$, The discrete dependent variable data points are $\lambda = [\lambda_1, \lambda_2, \dots, \lambda_n]$, The Fourier coefficients are $A = [\varpi, a_0, a_1, b_1, a_2, b_2, \dots, a_N, b_N]$. The Fourier series function is as follows :

$$\lambda_{fit}\left(S\right) = a_0 + \sum_{i=1}^{N}\left[a_i \cos\left(\varpi \cdot i \cdot S\right) + b_i \sin\left(\varpi \cdot i \cdot S\right)\right] \tag{5}$$

Where n is the number of test points,N is the order of the Fourier series.

The standard function fitting method uses the error least square method of data points. This paper uses the least square model to fit the curve. The fitting accuracy is determined by the determination coefficient R^2. The maximum value of R^2 is 1. The closer the value of R^2 is to1, the closer the fitting results are to the actual value. The calculation formula of the determination coefficient R^2 is as follows:

$$R^2 = 1 - \frac{\sum_{i=1}^{n}\left(\lambda_{fit}\left(S_i\right) - \lambda\left(S_i\right)\right)^2}{\sum_{i=1}^{n}\left(\lambda_{fit}\left(S_i\right) - \overline{\lambda\left(S_i\right)}\right)^2} \tag{6}$$

Where $\lambda_{fit}(S_i)$ is the calculated value of the fitting function, $\lambda(S_i)$ is the actual value, $\overline{\lambda(S_i)}$ is the average value.

Because the power-to-load transfer coefficient in the whole cycle constitutes a closed curve, which cannot be fitted by function, it is divided into upper and lower strokes to fit separately, as shown in Figure 3.

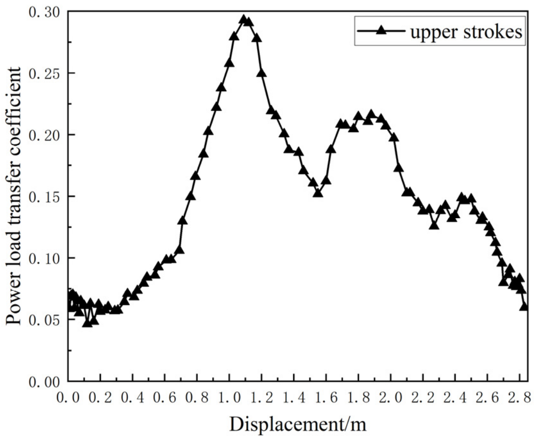

(a) Upper stroke power load transfer coefficient

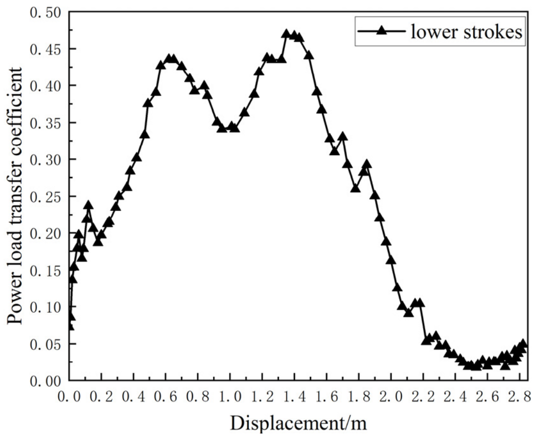

(b) Lower stroke power load transfer coefficient

Fig 3. Power load transfer coefficient curve

According to the equation (5), With the help of the MATLABR2022b curve fitting tool, the Fourier series fitting of different orders is carried out by increasing the order N. The relationship between the fitting order of Fourier series and the determination coefficient R^2 is shown in Figure 4. It can be seen from the figure that as the fitting order increases, the coefficient of determination R^2 is also increasing. That is, as the order increases, the Fourier series continues to approach the original coefficient curve. When the order is in 1~6, the coefficient of determination R^2 growth trend is obvious. When the order $\mathrm{N} = 6$, the determination coefficient R^2 of the upper and lower strokes reaches 99%. However, when $\mathrm{N} > 6$, R^2 does not increase. According to this feature, when R^2 reaches 99%, the iteration can be stopped to avoid the fitting equation being too complicated.

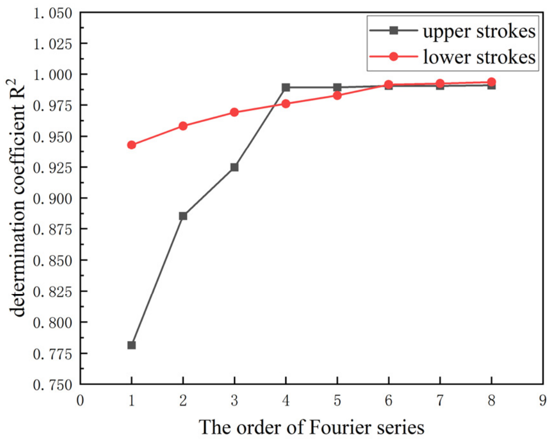

Fig 4. Relationship between the coefficient of determination and order

The above analysis shows that taking the 6th-order Fourier coefficient for fitting is reasonable. The 6-order Fourier series fitting results of the power-to-load transfer coefficient curves of the upper stroke and the lower stroke are shown in Figure 5. From the image trend, the overall is high-precision fitting.

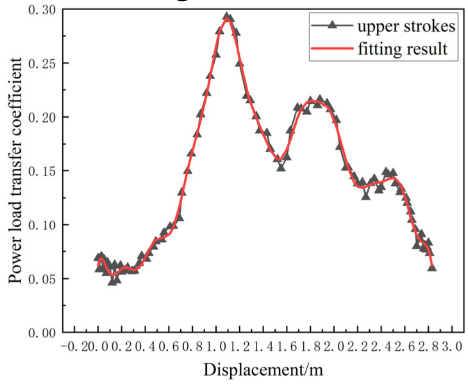

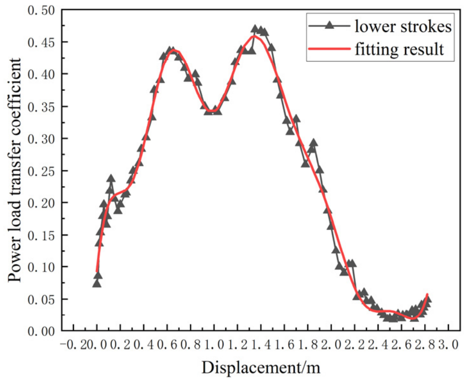

(a) Upper stroke fitting results (b)Lower stroke fitting results

Fig 5. Power load transfer coefficient curve fitting results

The expressions of the power-to-load transfer coefficient fitting curves $\lambda_{upfit1}(S)$ and $\lambda_{lowfit1}(S)$ of the upper stroke and the lower stroke are:

$$\begin{aligned}\lambda_{upfit1}(S)=0.152&-0.077\cos(2.22\cdot S)-0.009\sin(2.22\cdot S)\\&-0.009\cos(2\cdot 2.22\cdot S)-0.034\sin(2\cdot 2.22\cdot S)\\&+0.022\cos(3\cdot 2.22\cdot S)+0.007\sin(3\cdot 2.22\cdot S)\\&-0.023\cos(4\cdot 2.22\cdot S)-0.009\sin(4\cdot 2.22\cdot S)\\&+0.001\cos(5\cdot 2.22\cdot S)+0.001\sin(5\cdot 2.22\cdot S)\\&+0.003\cos(6\cdot 2.22\cdot S)+0.004\sin(6\cdot 2.22\cdot S)\end{aligned} \tag{7}$$

$$\begin{aligned}\lambda_{lowfit1}(S)=-0.228&-0.511\cos(1.501\cdot S)+0.805\sin(1.501\cdot S)\\&+0.049\cos(2\cdot 1.501\cdot S)+0.645\sin(2\cdot 1.501\cdot S)\\&+0.422\cos(3\cdot 1.501\cdot S)+0.296\sin(3\cdot 1.501\cdot S)\\&+0.283\cos(4\cdot 1.501\cdot S)-0.088\sin(4\cdot 1.501\cdot S)\\&+0.072\cos(5\cdot 1.501\cdot S)-0.165\sin(5\cdot 1.501\cdot S)\\&-0.003\cos(6\cdot 1.501\cdot S)-0.072\sin(6\cdot 1.501\cdot S)\end{aligned} \tag{8}$$

3. Indicator Diagram Inversion Verification

The data corresponding to the calibration process is removed from the measured data. And then, the electric power and suspension point displacement data of other cycles are substituted into Equations (7) and (8). The suspension point load in this period is calculated using the above method, and the indicator diagram is drawn. The measured indicator diagram and the inversion indicator diagram are shown in Figure 6(a). It can be seen from the graph that there is a significant error between the calculation of the suspension point load and the measured suspension point load in the partial. The error is most apparent in the dead point area, the loading-increasing line, and the loading-decreasing line. The error of the calculated load is shown in Figure 6 (b). The maximum error is 55%, and the error of 30% of the calculation points exceeds 10%. The accuracy of the inverted indicator diagram is insufficient to meet the engineering application.

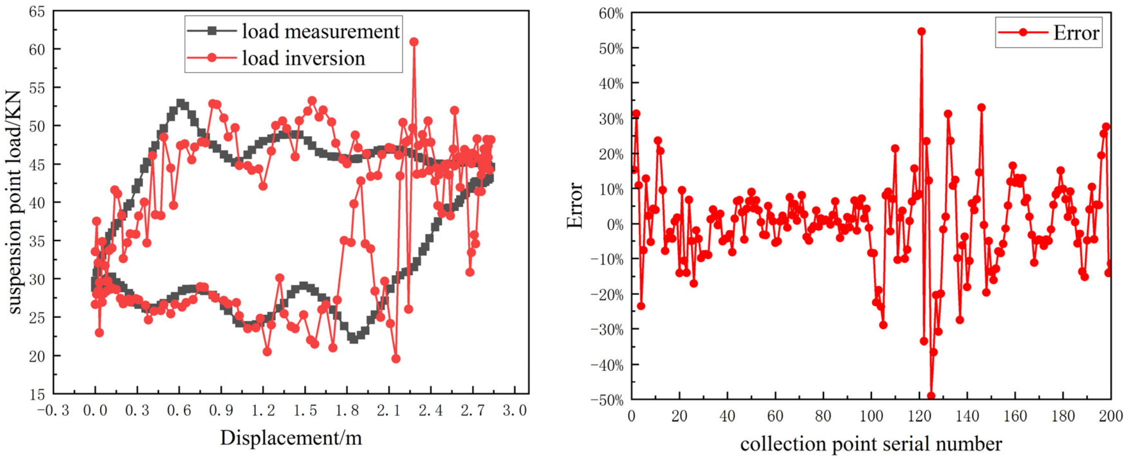

(a) Measured and inverted indicator diagram

(b)The error of load inversion value

Fig 6. Indicator diagram and error

3.1. Optimization of Power-to-load Transfer Coefficient

After analyzing the test data shown in Table 1, it is concluded that under the following conditions, the calculation of the suspension point load will have a large mutation or error: (1) At some measuring points, the electric power is small, but the load is large. There is an order-of-magnitude gap between the two, resulting in $\lambda(S_i)$ approaching zero. (2)Some pumping units with poor balance have reverse power generation during the downstroke. At this time, the instantaneous output power of the motor is negative. But when the motor has external positive power, the instantaneous power of the motor is positive. There must be a moment when the instantaneous output power of the motor is zero.

The above two cases will lead to $\lambda(S_i)$ equal to zero or close to zero. When calculating the suspension point load, $\lambda(S_i)$ is the divisor. The tiny error of $\lambda(S_i)$ causes the error of the calculated value of the suspension point load to be significantly amplified. To avoid the inversion accuracy being seriously affected by the above phenomenon. It is necessary to move the overall coefficient curve in the positive direction so that $\lambda(S_i)$ is far away from the zero-value region.

Based on this, the power amplification factor R and the axis shift pipette Q are introduced into the calculation formula of $\lambda(S_i)$. In order to make $\lambda(S_i)$ in a reasonable numerical range that is no longer zero or close to zero. As the following equation shows:

$$\lambda\left(S_i\right)=\frac{P_i\cdot R+Q}{W_i} \qquad i=1,\ldots,n \tag{9}$$

Where S_i is the suspension point displacement, m; P_i is the instantaneous motor output power, kW; W_i is the suspension point load, kN; $\lambda(S_i)$ is the power-to-load transfer coefficient at the ith measurement point.

In the inversion of the suspension point load, the parameters R and Q also need to be introduced, as shown in the following equation :

$$W_i^{'}=\frac{P_i^{'}\cdot R+Q}{\lambda\left(S_i\right)} \qquad i=1,\ldots,n \tag{10}$$

Where W_i' is the calculated value of load inversion, kN; P_i' is the instantaneous motor output power, kW.

In Equations (9), $\lambda(S_i)$ is calculated by randomly taking different values for parameters R and Q, where the power and load values are the data shown in table 1. The calculation results are shown in Figure 7. When $\mathrm{R}=1$ and $\mathrm{Q}=0$, the fluctuation and dispersion of the power load transfer coefficient at each measurement point are low. But $\lambda(S_i)$ is close to zero or equal to zero, which is not conducive to the inversion calculation of the suspension point load. When $R = 10$ and $Q = 50$, $\lambda(S_i)$ is much larger than zero, which is beneficial to the inversion calculation of the suspension point load. But the fluctuation and dispersion of the power-to-load transfer coefficient at each measurement point are high, which is not conducive to the load calculation in the whole cycle.

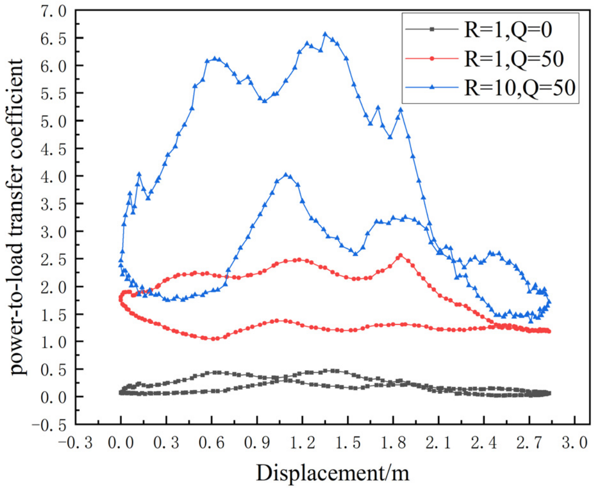

Fig 7. Power-to-load transfer coefficient curves under different values of parameters R and Q

To control the fluctuation and dispersion of the power load transfer coefficient and ensure that $\lambda(S_i)$ is far away from the zero-value region. The variance of the power-to-load transfer coefficient is taken as the objective function. The values of R and Q are optimized with the minimum variance as the goal. The optimal target function is shown as follows:

$$\sigma^2 = \min\left[\frac{1}{n}\sum_{i=1}^{n}\left(\frac{P_i \times R + Q}{W_i} - \frac{1}{n}\sum_{i=1}^{n}\frac{P_i \times R + Q}{W_i}\right)^2\right] \qquad i = 1,\dots,n \tag{11}$$

Based on the above requirements for the power-to-load transfer coefficient curve, the constrain of this optimization model are as follows:

$$\begin{cases} R \geq 1 \\ \min\left(\dfrac{P_i \times R + Q}{W_i}\right) \geq 1 \qquad i = 1,\dots,n \\ Q \geq 0 \end{cases} \tag{12}$$

The particle swarm optimization algorithm (PSO) is used to calculate this model. PSO is a swarm intelligence optimization technique. Much practical evidence shows that the algorithm is an effective optimization tool[20-22].

The process of the PSO algorithm is shown in Figure 8(a). The PSO algorithm first initializes a group of random particles, that is, an unexpected solution. Then the particle swarm follows the current optimal particle to search in the solution space, that is, to find the optimal solution through iteration. Suppose that the position and velocity of the *ith* particle in the D dimensional search space are respectively equal to:$X^i = (x_{i,1}, x_{i,2}, \dots, x_{i,d})$ and $V^i = (v_{i,1}, v_{i,2}, \dots, v_{i,d})$. The particle updates its value in each iteration by tracking the individual extremum and the optimal global solution. The particles update the velocity and position according to the following equation:

$$v_{i,j}(t+1) = wv_{i,j}(t) + c_1 r_1\left[p_{i,j} - x_{i,j}(t)\right] + c_2 r_2\left[p_{g,j} - x_{i,j}(t)\right] \tag{13}$$

$$x_{i,j}(t+1) = x_{i,j}(t) + v_{i,j}(t+1), j = 1,2,\dots,D \tag{14}$$

Where w is the inertia weight, c_1 is the self-learning factor, c_2 is the group learning factor, r_1 and r_2 are random numbers uniformly distributed between 0 and 1.

MATLABR2022b software is used to compile the particle swarm optimization algorithm. The number of particles is 50, the maximum number of iterations is 250, the inertia weight is 0.8, and the self-learning factor and the group-learning factor are 2. When the optimization iteration reaches the maximum number of iterations after 250 times, the optimization reaches a stable state. The calculated optimal values are $\mathrm{R} = 1, \mathrm{Q} = 48$. The value and the measured power and load data shown in Fig.2 (a) are substituted into Eq.(9) to calculate the power load transfer coefficient in this period. The calculation results are shown in Figure 8(b).

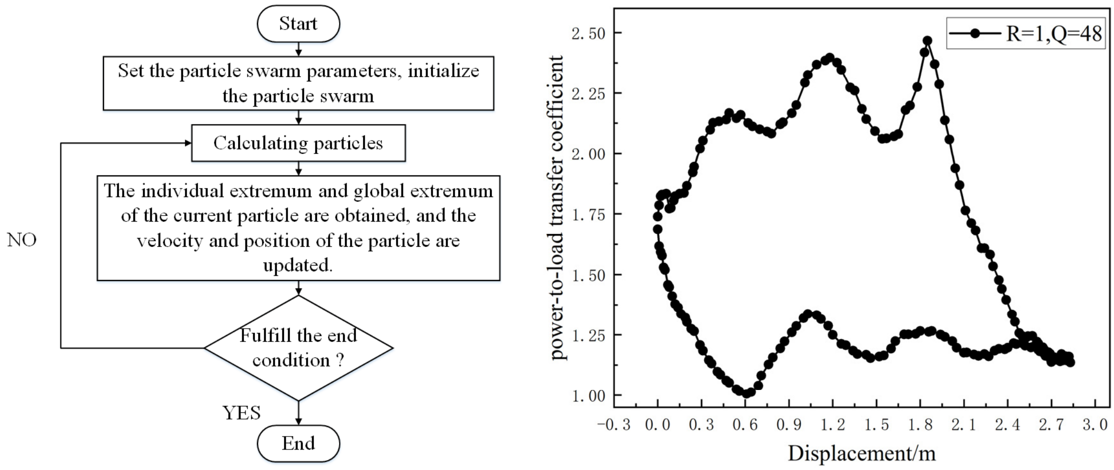

(a) The process of the PSO algorithm (b) Optimization curve of power-to-load transfer coefficient

Fig 8. The PSO algorithm process and the optimized coefficient

3.2. Results Comparison

The curve in Fig.8(b) is also divided into up and down strokes. Fourier series are also used for function fitting. When the order of the Fourier series is 5, the determination coefficient of the fitting reaches 99%. The fitting results are shown in Figure 9.

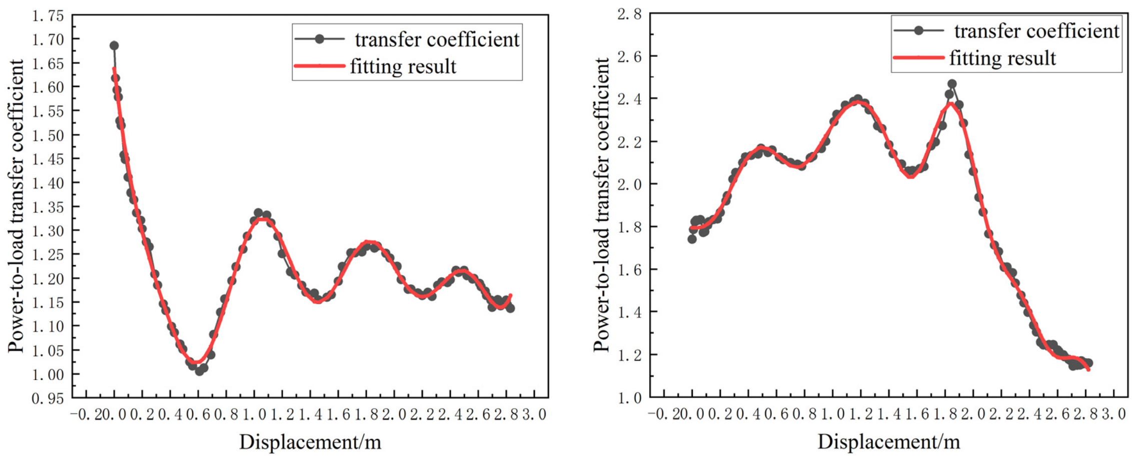

(a) Fitting results of upper stroke (b) Fitting results of lower stroke

Fig 9. The fitting results of the transfer coefficient

The expressions of the power-to-load transfer coefficient fitting curves $\lambda_{upfit2}(S)$ and $\lambda_{lowfit2}(S)$ of the upper stroke and the lower stroke are:

$$\begin{aligned}\lambda_{\mathrm{up}fit2}(S) &= 1.59+0.49\cos(1.56\cdot S)-0.53\sin(1.56\cdot S)\\ &-0.02\cos(2\cdot 1.56\cdot S)-0.61\sin(2\cdot 1.56\cdot S)\\ &-0.27\cos(3\cdot 1.56\cdot S)-0.25\sin(3\cdot 1.56\cdot S)\\ &-0.14\cos(4\cdot 1.56\cdot S)+0.06\sin(4\cdot 1.56\cdot S)\\ &-0.01\cos(5\cdot 1.56\cdot S)+0.12\sin(5\cdot 1.56\cdot S)\end{aligned} \tag{15}$$

$$\begin{aligned}\lambda_{\mathrm{low}fit2}(S) &= 1.89-0.28\cos(1.93\cdot S)+0.41\sin(1.93\cdot S)\\ &+0.12\cos(2\cdot 1.93\cdot S)+0.14\sin(2\cdot 1.93\cdot S)\\ &+0.17\cos(3\cdot 1.93\cdot S)-0.05\sin(3\cdot 1.93\cdot S)\\ &-0.05\cos(4\cdot 1.93\cdot S)+0.04\sin(4\cdot 1.93\cdot S)\\ &+0.04\cos(5\cdot 1.93\cdot S)-0.09\sin(5\cdot 1.93\cdot S)\end{aligned} \tag{16}$$

Based on the measured data shown in Figure 6, the power-to-load transfer coefficient is calculated by Equation (15) and Equation (16). The suspension point load is calculated according to the above method. The indicator diagram inversion results are shown in Figure 10(a). The comparison of the inversion indicator diagrams before and after the optimization of the power load transfer coefficient is shown in Figure 10(b). It can be seen from the figure that the accuracy of the inverted indicator diagram is improved after the coefficient is optimized.

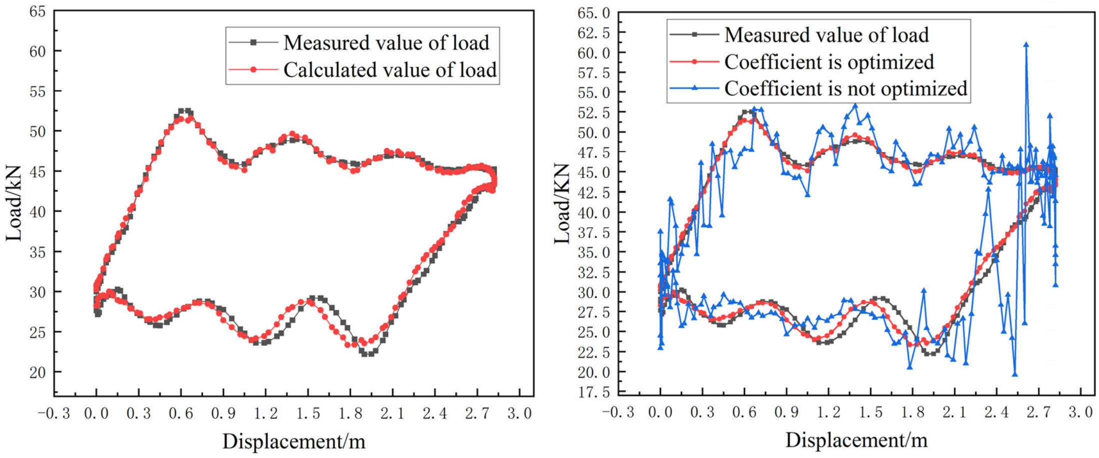

(a)The results of indicator diagram inversion(b)Comparison before and after coefficient optimization

Fig 10. Comparison of indicator diagram results

To measure the accuracy of the indicator diagram inversion by the power load coefficient method. This paper selects the "coincidence rate definition method" required by the oilfield site to calculate the accuracy[23]. The "coincidence rate definition method" calculation process is as follows: Firstly, the error between the inversion value and the measured value of the suspension point load is calculated. Then, the coincidence rate of each acquisition point is calculated, and the coincidence rate of the acquisition points in the whole cycle is averaged. The average value is the coincidence rate of the inversion indicator diagram. The specific formula is as follows:

$$\beta(S_i)=1-\frac{\left|w_1(S_i)-w_2(S_i)\right|}{w_1(S_i)} \tag{17}$$

$$\beta_{avg}=\frac{\sum_{i=1}^{n}\beta(S_i)}{n} \tag{18}$$

$$\beta_{\min} = \left[1 - \frac{\left| w_1\left(S_i\right) - w_2\left(S_i\right) \right|}{w_1\left(S_i\right)} \right]_{\min} \tag{19}$$

Where $w_1(S_i)$ is the measured load value of different acquisition points ; $w_2(S_i)$ is the inversion load value of different acquisition points ; $\beta(S_i)$ is the coincidence rate prediction indicator diagram at different acquisition points ; β_{avg} is the average coincidence rate of the predicted indicator diagram ; β_{min} is the minimum coincidence rate for the prediction indicator diagram. The standard coincidence rate definition method is shown in Table 2.

Table 2. Coincidence rate definition standard

Level	Excellent	Good	Poor
β_{avg}	$\beta_{avg} > 95\%$	$95\% \geq \beta_{avg} \geq 90\%$	$\beta_{avg} < 90\%$
β_{min}	$\beta_{min} > 90\%$	$\beta_{min} \geq 85\%$	$\beta_{min} < 85\%$

The coincidence rate of each measurement point in the inverse indicator diagram is shown in Figure 11. The average coincidence rate of the inversion indicator diagram without the optimized coefficient is 91%, and the minimum coincidence rate of each measurement point is 45%. The average coincidence rate of the inversion indicator diagram with the optimized coefficient is 98%, and the minimum coincidence rate of each measurement point is 91%. According to the coincidence rate judgment standard, the accuracy of the inversion indicator diagram obtained by the optimized power load transfer coefficient method is excellent, and the inversion accuracy is much higher than the results before optimization.

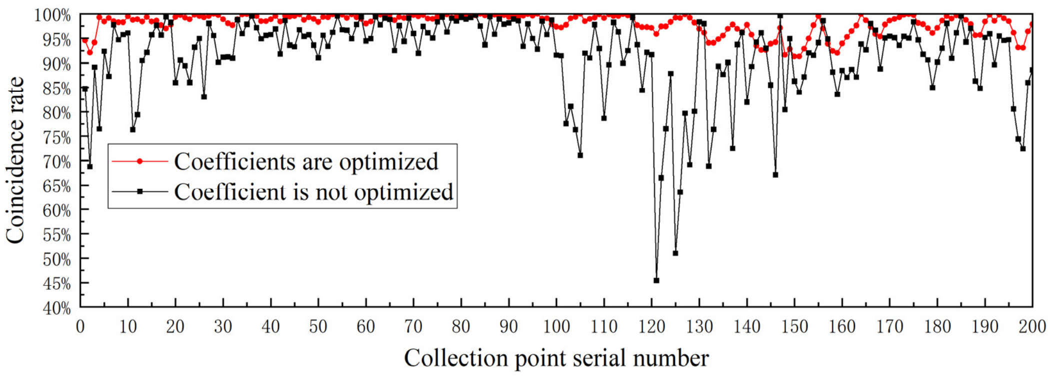

Fig 11. The coincidence rate of the inversion indicator diagram

4. Summary

(1) A new method based on the power-to-load transfer coefficient inversion indicator diagram is proposed by analyzing the principle of the electrical parameter inversion indicator diagram. The practical application process of this method is more straightforward, and the accuracy is higher.

(2)The Fourier series fits the power-to-load transfer coefficient. High fitting accuracy is obtained, and the fitting equation is relatively simple. The fitted power-to-load transfer coefficient equation is used for indicator diagram inversion. The average coincidence rate of the inversion indicator diagram is 98%, and the evaluation result of the coincidence rate definition method is excellent.

(3)To avoid the significant error of the calculated load when the power-to-load transfer coefficient approaches zero, t the power amplification factor R and the axis shift pipette Q are introduced. The result of the model obtained by the particle swarm optimization algorithm is $\mathrm{R} = 1, \mathrm{Q} = 48$. The optimized power load transfer coefficient can significantly improve the load calculation accuracy. The average coincidence rate of the inversion indicator diagram without the optimized coefficient is 91%, and the minimum coincidence rate of each measurement point is 45%. The average coincidence rate of the inversion indicator diagram with the optimized coefficient is 98%, and the minimum coincidence rate of each measurement point is 91%.

The method of inversion of suspension point indicator diagram based on the power-to-load transfer coefficient proposed in this paper has the following characteristics compared with the current method: the inversion accuracy is significantly improved, the process is simpler, no need to monitor the parameters of the pumping unit. It provides a new method for the engineering application of an electrical parameter inversion indicator diagram.

References

[1] Wang, A (Wang, An);Gong, GL (Gong, Guoliang);Shen, RX (Shen, Rongxuan);Mao, WY (Mao, Wenyu); Lu, HX (Lu, Huaxiang);Wang, K (Wang, Ke);Wang, JP (Wang, Junping).Tracking the multi-well surface dynamometer card state for a sucker-rod pump by using a particle filter[J].IET Communications, 2018,Vol.12(16): 2058-2.

[2] Manzhou Cai. Development of Real time Monitoring System for Electric Power of Pumping Unit Wells [J]. Journal of Jianghan Petroleum Institute,2003,(3): 120-121.

[3] Dechun Cheng,Lv Fei, Yao Ya, Liangfei Xiao, et,alA NEW MODEL BASED ON THE ELECTRICAL DIAGRAMS FOR DIAGNOSING THE WORKING STATUS OF BELT-PUMP-UINT WELLS [J]. Daqing Petroleum Geology and Development,2017,Vol.36 (5): 119-123.

[4] Gibbs, S.G.Utility of Motor-Speed Measurements in Pumping-Well Analysis and Control[J].SPE Production Engineering,1987, Vol.2(3): 199-208.

[5] Li Hujun, Li Ying, Long Qiansheng, Zhi Lianyou. Calculate the dynamometer diagram of a pre pumping unit well using the measured power curve [J]. oil field equipment,1992,(5): 33-37.

[6] Zheng, BY (Zheng, Boyuan); Gao, XW (Gao, Xianwen); Li, XY (Li, Xiangyu).Fault detection for sucker rod pump based on motor power.[J]. Control Engineering Practice,2019, Vol. 86: 37-47.

[7] Zhang Shirong, Li Changxi. Indirect measurement of indicator diagram for beam pumping unit [J]. Journal of Huazhong University of Science and Technology (Natural Science Edition),2004,Vol.32 (11): 62-64.

[8] Chen Peiyi, Yao Chundong, Dong Shimin, Yao Hongtian. Simulation Model of Polished Rod Indicator Diagram Based on Measured Electrical Power of Pumping Unit [J]. petroleum machinery, 2013,Vol. 41 (11): 91-95.

[9] Lv Zhizhong, Jiang Cheng, Jiang Lin, Zhong Gongxiang. Study on the Test System of Oil Pumping Machine Diagram Based on Electric Power [J]. Mechanical Design and Manufacturing,2019,(3): 225-228.

[10] Xiaoju Yin; Zhiliang Du; Yuxin Wang; Shiyu Lu; Yunxiang Li; Tingting Zhao.Analysis and experimental study of oil well indicator diagram based on electric parameter method[J].Energy Reports, 2022, Vol.8: 734-745.

[11] Wei, JL (Wei, Jingliang);Gao, XW (Gao, Xianwen).Electric-Parameter-Based Inversion of Dynamometer Card Using Hybrid Modeling for Beam Pumping System.[J].Mathematical Problems in Engineering, 2018, Vol.2018(1): 1-12.

[12] Wang Weijiang, Shi Yueting, Liu Jianyan, Ren Guishan, Dong Hanyuan. Neural network-based load inversion algorithm for electrical parameters [J]. Journal of Beijing Institute of Technology, 2015, Vol. 35(7): 706-710.

[13] Xishun Zhang;Junfeng Shi;Ruidong Zhao;Dakui Sun;Xin Zhang;Feng Deng;Yi Peng;Shiwen Chen;Haoyuan Chu;Qing Dong.Research and Application of Electric Power Curve Inversing Dynamometer Diagram Technology Using Big Data Approach[A].SPE Symposium: Production Enhancement and Cost Optimisation[C],2017.

[14] Ke Wang; Guoliang Gong; Rongxuan Shen; An Wang; Zhaolin Yao; Wenyu Mao; Huaxiang Lu.Novel physical network algorithm for indirect measurement of polished rod load of beam-pumping unit[J].The Journal of Engineering,2019, Vol. 2019(10): 7287-7292.

[15] Yi Peng.Artificial Intelligence Applied in Sucker Rod Pumping Wells: Intelligent Dynamometer Card Generation, Diagnosis, and Failure Detection Using Deep Neural Networks[A].SPE Annual Technical Conference and Exhibition[C],2019.

[16] Dandan Zhu; Xiaoting Luo; Zhanmin Zhang; Xiangyi Li; Gao Peng; Liping Zhu; Xuefeng Jin.Full Reproduction of Surface Dynamometer Card Based on Periodic Electric Current Data[J].SPE Production & Operations,2021,Vol.36(3): 594-603.

[17] Yong, R (Yong, Rui);Ye, J (Ye, Jun);Li, B (Li, Bo);Du, SG (Du, Shi-Gui).Determining the maximum sampling interval in rock joint roughness measurements using Fourier series[J].International Journal of Rock Mechanics and Mining Sciences,2018, Vol.101: 78-88.

[18] Yang, ZY (Yang, ZY);Di, CC (Di, CC);Yen, KC (Yen, KC).The effect of asperity order on the roughness of rock joints[J].International Journal of Rock Mechanics and Mining Sciences,2001, Vol.38(5): 745-752.

[19] Yang, ZY (Yang, ZY);Lo, SC (Lo, SC);Di, CC (Di, CC).Reassessing the Joint Roughness Coefficient (JRC) Estimation Using Z_2[J].Rock Mechanics and Rock Engineering,2001, Vol.34(3): 243-251.

[20] Xiaohong Li;Shuanghe Yu.Three-dimensional path planning for AUVs in ocean currents environment based on an improved compression factor particle swarm optimization algorithm[J]. Ocean Engineering,2023, Vol.280: 114610.

[21] Ke Ren;Lu Jia;Jiantao Huang;Min Wu.Research on cutting stock optimization of rebar engineering based on building information modeling and an improved particle swarm optimization algorithm [J]. Developments in the Built Environment,2023, Vol.13: 100121.

[22] Junjun Jiao;Jiulong Cheng;Yuben Liu;Haiyan Yang;Dingrui Tan;Peng Cheng;Yuqi Zhang;Chenglin Jiang;Zhi Chen.Inversion of TEM measurement data via a quantum particle swarm optimization algorithm with the elite opposition-based learning strategy[J].Computers & Geosciences,2023, Vol. 174: 105334.

[23] Cao Sheng. Comparative study on power reverse demonstration power diagram of pumping machine based on mechanism and data [D]. China University of Petroleum (Beijing),2021.